JOURNAL OF AIRCRAFT
Vol. 51, No. 2, March–April 2014

Nature of Freeplay-Induced Aeroelastic Oscillations

Denis B. Kholodar*
Bombardier Aerospace, Ville Saint-Laurent, Québec H4S 2A9, Canada

DOI: 10.2514/1.C032295

Time- and frequency-domain analyses are used to revisit a well studied case of an aeroelastic wing with control-surface freeplay nonlinearity. The dynamic response in general is presented as dependent on the stability of two linear systems, with zero and nominal control-surface rotational stiffness, and values of two angles, freeplay and preload. The principal new findings include the following. A physical explanation is given to the bifurcation airspeeds and frequencies of the oscillations for the system with both zero and nonzero aerodynamic preload of the control surface. For the latter and more complex case, it is shown and explained why a certain amount of the preload is not only always destabilizing but may also be the reason for the otherwise unexpected higher-frequency oscillations. A conclusion thus is drawn that the aircraft control-surface freeplay analyses based only on zero and high quenching aerodynamic preloads are nonconservative. All results are compared with the experimental and other published theoretical analyses for the considered model. Finally, a suggestion is given for future experiments with a goal to observe the response changes with the preload and to determine the stabilizing control-surface hinge moment.

Nomenclature

h	=	plunge displacement of the wing
K_{equiv}	=	equivalent control-surface rotational stiffness in the describing function method
k	=	reduced frequency
q_i	=	modal coordinate
U	=	airspeed
U_f	=	flutter airspeed
α	=	pitch angle of the wing
β	=	control-surface rotational angle
δ	=	freeplay region
δ_{PL}	=	preload of the control surface
$\varphi_{\beta i}$	=	modeshape matrix component

I. Introduction

EARLY studies conducted with the Duke University aeroelastic wing model with a control-surface freeplay resulted in significant advances in understanding the nonlinear dynamics of this problem. The abundant experimental data collected over the years served as a validation test case to a number of computational codes. The following is a brief review of the most prominent publications with that model.

Figure 1 shows a photograph of the wing. It is a rectangular NACA 0012 wing that has three degrees of freedom (DOFs): plunge, pitch about the quarter-chord axis, and control-surface rotation about the three-quarter-chord axis. The control surface (CS) restoring moment has freeplay, a region of zero CS rotational stiffness. The freeplay implementation is shown in Fig. 2. Outside the freeplay, the CS has nominal or, in aircraft terminology, fully operative rotational stiffness.

The initial experimental and theoretical investigation was presented in Conner et al. [1]. The equations of motion in [1] were based on Theodorsen's derivation [2]. To be able to simulate arbitrary motion of the system in the time domain, the state–space form of Edwards et al. [3] using two "augmented" states for Jones's approximation of the Wagner function were employed in [1]. Five regions of the response were classified based on the time-domain simulation. The scalability of the response amplitude with the freeplay as well as the independence of the limit cycle oscillations (LCOs) bifurcation airspeeds with the freeplay were established.

In Tang et al. [4], the unsteady time domain aerodynamic forces were based on Peters and Johnson's [5] and Peters and Cao's [6] finite-state model with augmented aerodynamic lag states. The describing function method (DFM), i.e., the harmonic balance method (HBM) retaining the fundamental harmonic, was used in [4] alongside the time-domain simulations. Good agreement between the two approaches was observed. The use of the DFM provided significant insights not readily available from the time-domain analysis. Among them was the determination of the minimal airspeed and the initial conditions required to observe LCO. Unstable LCO were identified, and their relationship to the effect of the initial conditions was better understood.

Chen and Sulaeman [7] used this problem as one of the validation cases for the generalized direct simulation method discrete-time domain state–space approach developed in the ZONA program to simulate transient response of open- and closed-loop nonlinear aeroelastic systems. The three-dimensional method ZONA6 was used to generate the frequency-domain unsteady air loads that were made two-dimensional and transformed to the time domain using Rogers's rational function approximation (RFA) [8].

The HBM analysis was extended in Liu and Dowell [9] by retaining higher harmonics. The analytical model used was similar to the one in [1]. It was concluded that, generally but not always, retaining more harmonics results in the improvement of the DFM results.

Trickey et al. [10] performed the experiments with the same model and applied the latest techniques of the nonlinear dynamical systems theory to characterize the motion of the system. The theoretical model followed [1]. The experimental and numerical bifurcation diagrams and spectrograms were obtained and compared. The effect of the initial conditions was studied. Experimental and theoretical stability of the LCO was considered from a local and global perspective. Certain basins of attractions were identified.

The Navier–Stokes and Euler aerodynamics were applied to this system in Kuruvila et al. [11] in time-accurate simulations. The work served as a limited validation of the modified CFL3D program code originally developed by NASA Langley Research Center and used at Boeing with the aim to simulate aircraft control-surface freeplay response in transonic regimes in industrial use. Most of the conclusions concerned the use of the computational fluid dynamics (CFD) aerodynamic solver in such calculations. Contrary to all other analyses, it was observed that the amplitude of the response did not scale with the size of the freeplay, and the results were affected by the time-step size. This demonstrates the caution one needs in evaluation of CFD codes. The authors should be commended for carrying out this investigation.

Received 1 February 2013; revision received 30 July 2013; accepted for publication 13 August 2013; published online 26 February 2014.

*Engineering Specialist, Dynamics. Member AIAA.

Fig. 1 Photograph of the wing in the wind tunnel.

In Gordon et al. [12], the application of the DFM to obtain LCO amplitude and frequency was detailed further and automated. The two-dimensional incompressible unsteady (Theodorsen) aerodynamic forces from finite-element code ATLAS were imported into another Boeing proprietary program, Apex, to perform nonlinear response calculations. A locally parameterized continuation method was used to track accurately all flutter modes. Limit-cycle stability was assessed by examining the change in growth rate due to amplitude perturbations at a given airspeed. A companion time-domain analysis was also performed in Apex using Rogers's RFA transformation with five lag states of the frequency-dependent unsteady air loads. It was concluded that the agreement between the frequency- and time-domain analyses was quite good and that it was also improved in comparison with [4]. However, the theoretical results in [12] did not always agree well with the experiment.

Preload in a freeplay study was introduced in [13]. As shown in Fig. 2b, the preload is "assumed to act on the system so that the equilibrium position lies at some point on the linear arm". The change in the CS equilibrium can be caused by the changes in the airflow about the CS due to, for example, a change in Mach number or the angle of attack (AoA). The aircraft certification standards require very tight CS freeplay limits (a fraction of a degree). Maintaining such limits is challenging. Allegedly, there are known examples of aircraft with significant CS freeplay when no vibration was experienced in flight. Such occurrences may be explained by the presence of a sufficient amount of aerodynamic preload. For example, Chen and Lee [14] concluded that such loading of the horizontal tail was the probable reason why "F-16 was observed having a 6-time free-play angle of the MIL-spec limit, but no LCO occurred during the flight."

Recently, a study has been conducted by Tang and Dowell [15] with the same model for various AoA with and without gust excitation. With respect to the AoA part of their work, it was concluded that 1) the response of the system was sensitive to the AoA and initial conditions used; 2) the jump from the lower-frequency oscillation to a higher-frequency oscillation was affected by the AoA; 3) a certain AoA reducing the airspeed range of LCO was observed for the two experiments and numerical simulations with different freeplay; and 4) similar to the case of zero AoA, the system response scales with the freeplay.

The goal for revisiting the case originally presented in [1] in this work is to contribute to the explanation of 1) the sudden changes in the dynamic behavior observed in the previous studies, and 2) the values of the LCO frequencies as well as the bifurcation airspeeds (i.e., the airspeeds when the system behavior changes in character). Considering the effect of the AoA, the goal is to show and explain why the oscillations, in fact, grow in amplitude with the preload or AoA before becoming quenched by the substantial amount of the preload.

II. Theoretical Models Used Here

In the current work, two models of the system are employed. They are summarized in Table 1 and depicted in Fig. 3. The first model is identical to the one used in [1]. In this model, the airfoil aerodynamic

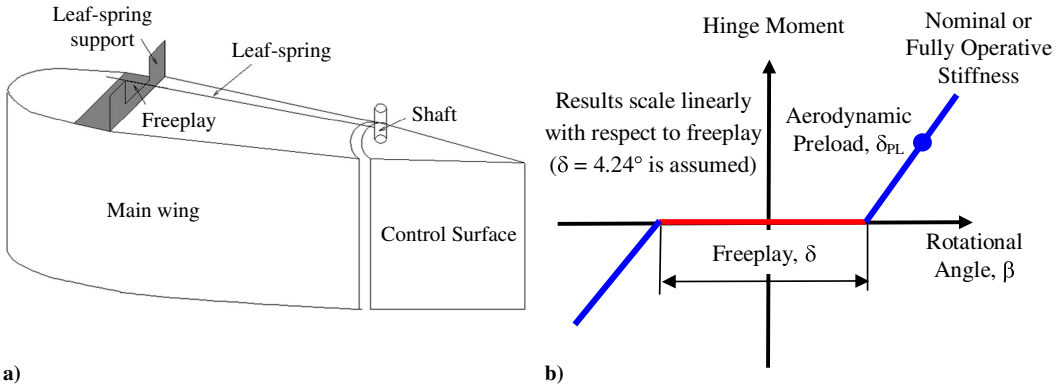

Fig. 2 Freeplay experimental model and theoretical idealization.

Table 1 Highlights of the theoretical models employed here

	Theodorsen model	Doublet-lattice model
Modal coordinates	Pitch, α	$q_1(\alpha, \beta, h)$
Modal coordinates	CS, β	$q_2(\alpha, \beta, h)$
Modal coordinates	Plunge, h	$q_3(\alpha, \beta, h)$
DOF containing freeplay	β	$\beta = \varphi_{\beta 1} \cdot q_1 + \varphi_{\beta 2} \cdot q_2 + \varphi_{\beta 3} \cdot q_3$
Aerodynamics	Theodorsen (k, α, β, h) [2]	Doublet-lattice (k, q_1, q_2, q_3) [16]
Transformation to time domain	Duhamel integral of Jones's approximation to Wagner's function, two augmented states [3]	Rogers's RFA [8], two lag terms.
State–space dimension	8×8	12×12
Integration scheme	Fourth-order Runge–Kutta	
Determination of freeplay end points	Henon's method [17]	Adaptive step

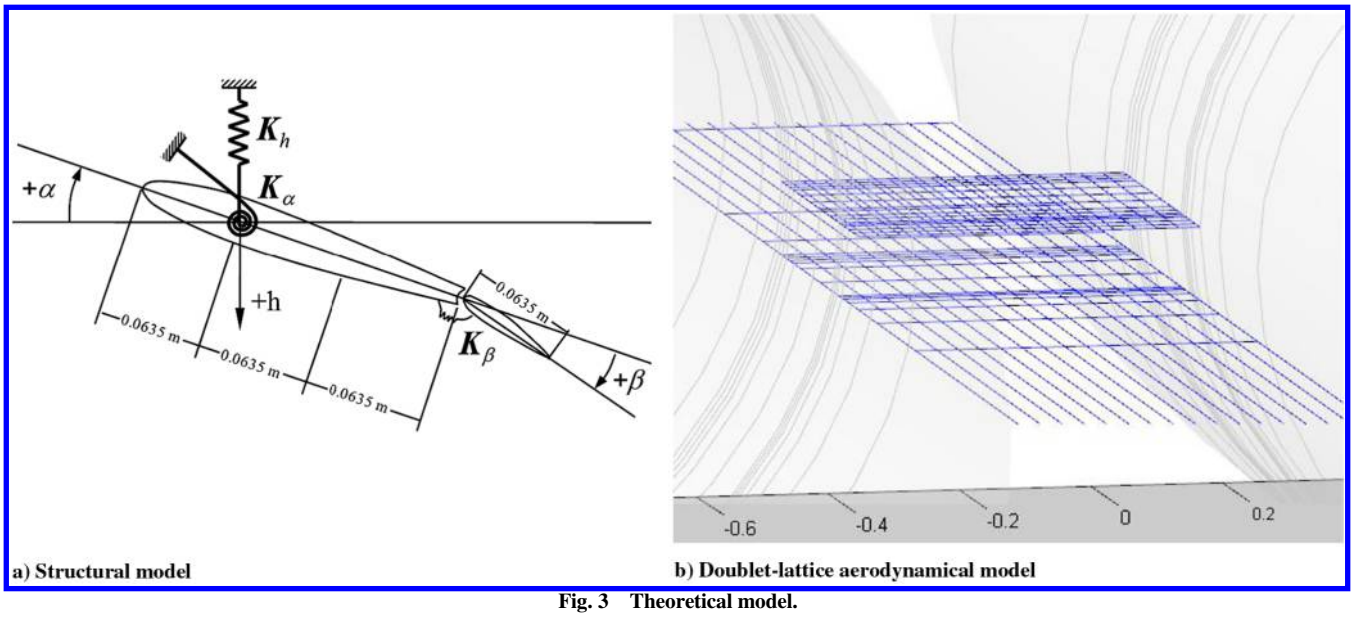

Fig. 3 Theoretical model.

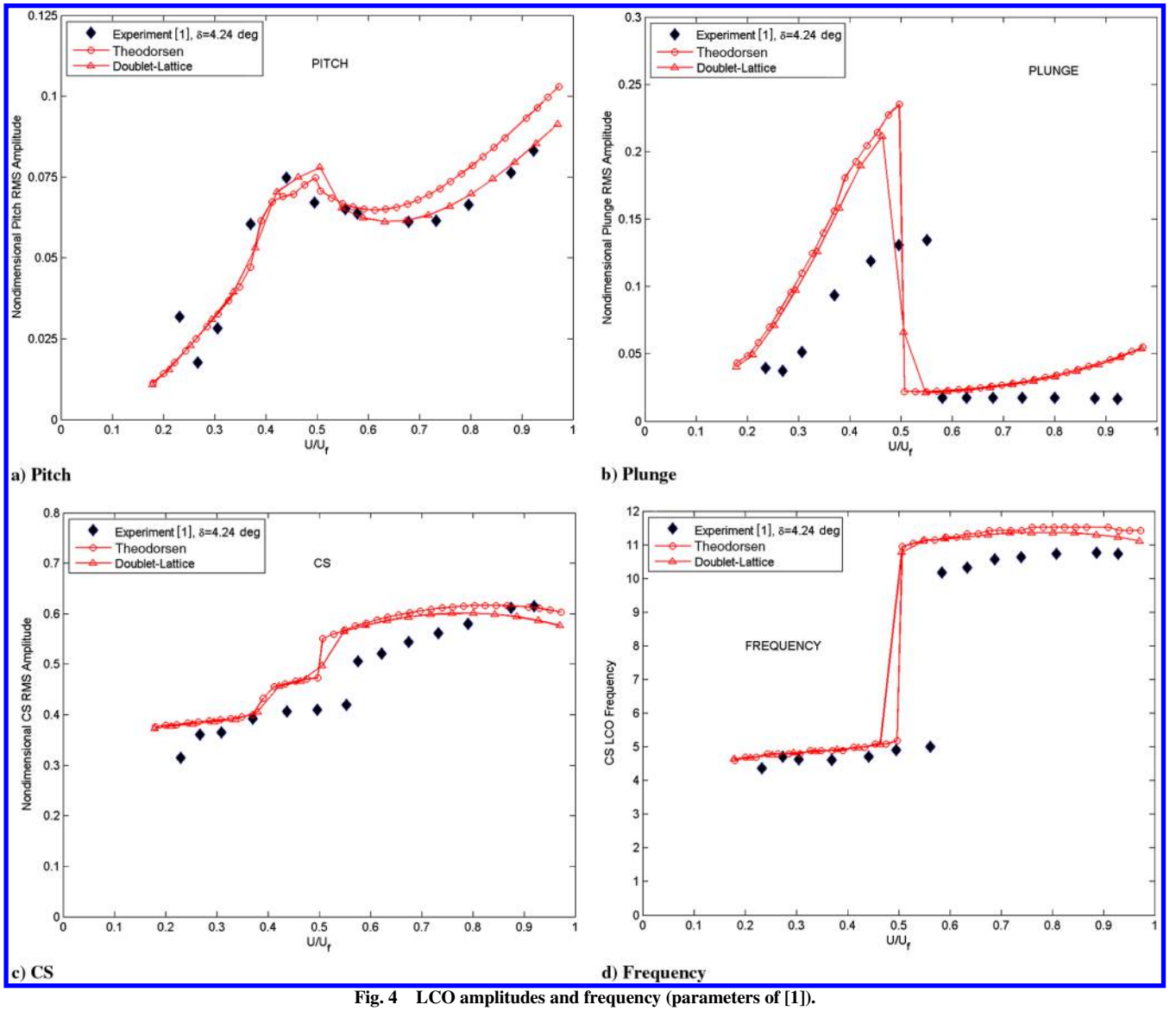

Fig. 4 LCO amplitudes and frequency (parameters of [1]).

moments and lift are explicitly given for the pitch, CS, and plunge DOF by Theodorsen in [2]. The unsteady generalized aerodynamic forces of the second model are obtained with the doublet-lattice method in MSC.Nastran [16]. Four aerodynamic panels were used: two representing the wing main and control surfaces and two representing the wind-tunnel walls that are parallel to the wing (only one of the latter panels is shown in Fig. 3b to not block the view). The other two wind-tunnel walls were modeled by the slender and interference bodies of a large diameter. Two optimized lag terms were used in the RFA transformation of the aerodynamic forces of this model. An inclusion of additional lag terms led to insignificant variations in the results.

The second model is used in the routine CS freeplay analyses of Bombardier aircraft. The aerodynamic forces in such analyses can be either scaled to match the CFD or wind-tunnel steady-state data or be replaced by the CFD unsteady aerodynamic forces. In aircraft finite-element models, the freeplay nonlinearity is modeled in the CS hinge DOF (i.e., not in one of the modal coordinates as in the Theodorsen model). For these two reasons, one may call the doublet-lattice model as the more general of the two.

In addition to these analyses, the DFM capable of accounting for the preload was also sparingly used. Finally, the time- and frequency-domain analyses were supplemented by the flutter trends (i.e., the evolution of the eigenvalues of the flutter determinant with the airspeed). The system parameters can be found in [1,15].

III. Results

A. Zero Preload

For clarity, the system response frequency and rms amplitudes as function of the normalized airspeed are presented twice. First, in Fig. 4, the results are shown only for the two theoretical models considered here and one set of the experimental results. (The experimental data were not available; thus, they were taken from the figures of other publications.) Second, in Fig. 5, all published time-domain results for this model are presented. The following effort was made to unite those data. The experimental and theoretical results of Conner et al. [1] together with the ZONA program predictions were taken as images from [7], courtesy of P. C. Chen. The digitized results of [4,11,12] and current results were then plotted on top of these images. The same experimental data contained in [4,11,12] were used as checks of the process. Published nominal flutter airspeeds were used to normalize the airspeed as was done in [1]. For the theoretical models considered here, these airspeeds were $U_f = 23.65$ m/s for the Theodorsen model and $U_f = 23.70$ m/s for the doublet-lattice model. The nondimensionalization of the response as adopted

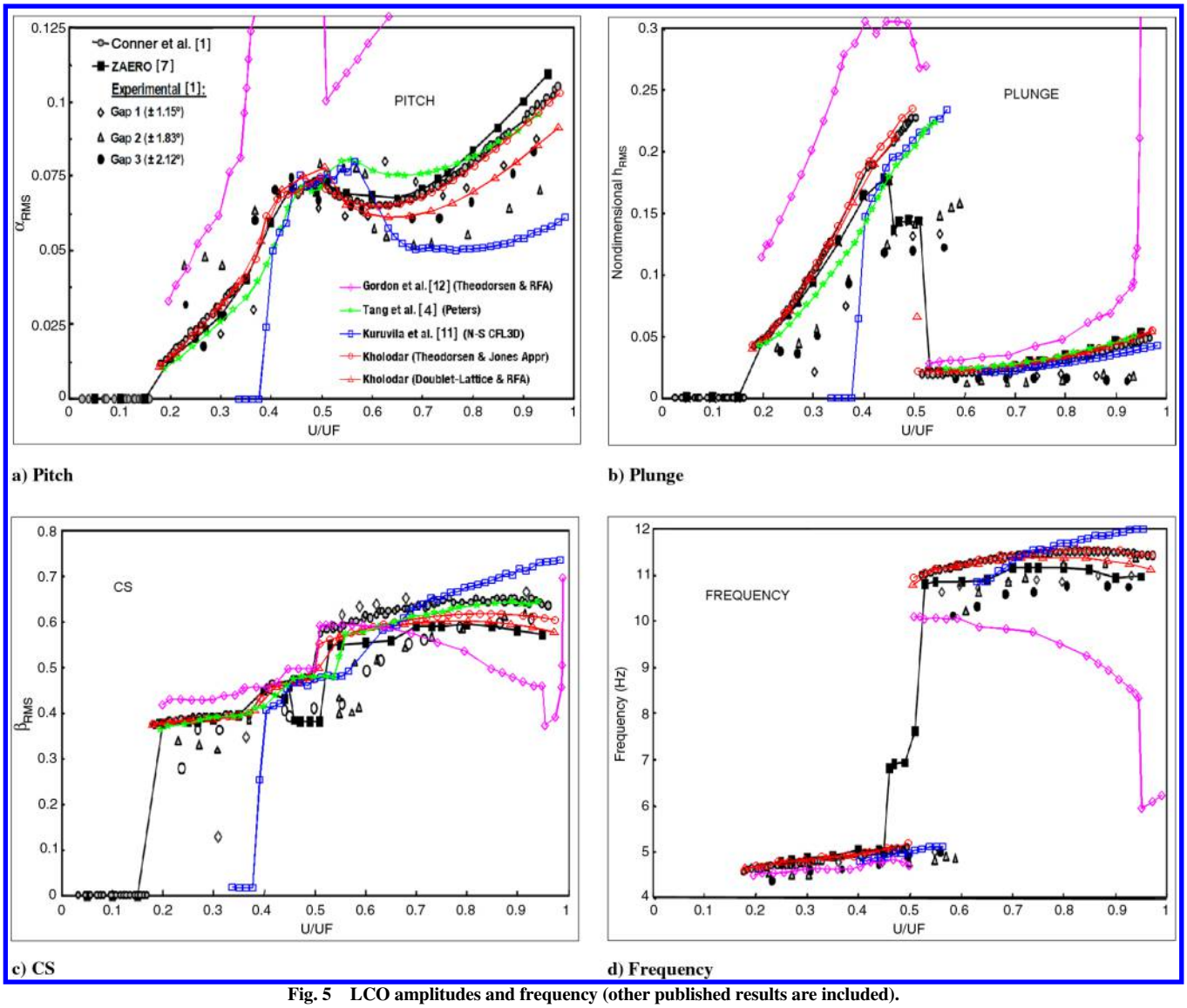

Fig. 5 LCO amplitudes and frequency (other published results are included).

originally in [1]: "the amplitude data have been normalized by the size of the freeplay region and by the airfoil semichord, in the case of the plunge data" has been since used in many subsequent studies including the experiments of [15]. The size of the freeplay region is $\delta = 4.24$ deg, and the semichord is 0.127 m. It can be concluded from Figs. 4 and 5 that the two current models produced adequate results matching the better among other theoretical predictions. The Theodorsen model values are very similar to those of [1] because these are identical models. The doublet-lattice model appears to better match experimental pitch amplitudes at higher airspeeds. Hidden behind the rms data is the variety of oscillatory behavior that is discussed next.

The oscillatory response of the system is now well known. An excellent graphical presentation of the distinct regions of oscillatory behavior can be found in [11]. The following most recent classification of the regions observed was given in [12]:

> "As shown by Conner, Conner et al., and Tang et al., there are four distinct regions of oscillatory behavior for flow speeds less than the flutter speed ($U_f = 23.9$ m/s for Conner's analysis). For velocities $0 < U < 0.18U_f$, any initial disturbance produces oscillations that decay to 0 amplitude fairly quickly (i.e., the system is well damped and stable). At $U \approx 0.18U_f$, there is a discrete jump from the rest state (global steady state) to a low-frequency limit cycle characterized by simple periodic oscillations in the control surface degree of freedom β. The system exhibits the simple low-frequency behavior until a speed $U \approx 0.32U_f$. Here, the system enters a transition region that consists of a more complex periodic low-frequency limit cycle. Several types of nonlinear behavior are present in the transition region including quasi-periodicity. The transition region exhibits increasing amplitudes in all three degrees of freedom as the flow speed increases. At a flow speed $U \approx 0.50U_f$, there is another abrupt change in the system behavior. The low-frequency limit cycle suddenly becomes unstable, and the system is attracted to a stable, high-frequency limit cycle. There is a dramatic drop in the plunge amplitude at this point. The pitch amplitude also drops and then grows again as the flow speed increases whereas the flap amplitude jumps in magnitude and then remains fairly constant. Also, the high-frequency flap motion returns to a simple periodic-type oscillation. Shortly after onset of this high-frequency limit cycle oscillation, the transient oscillations exhibit the

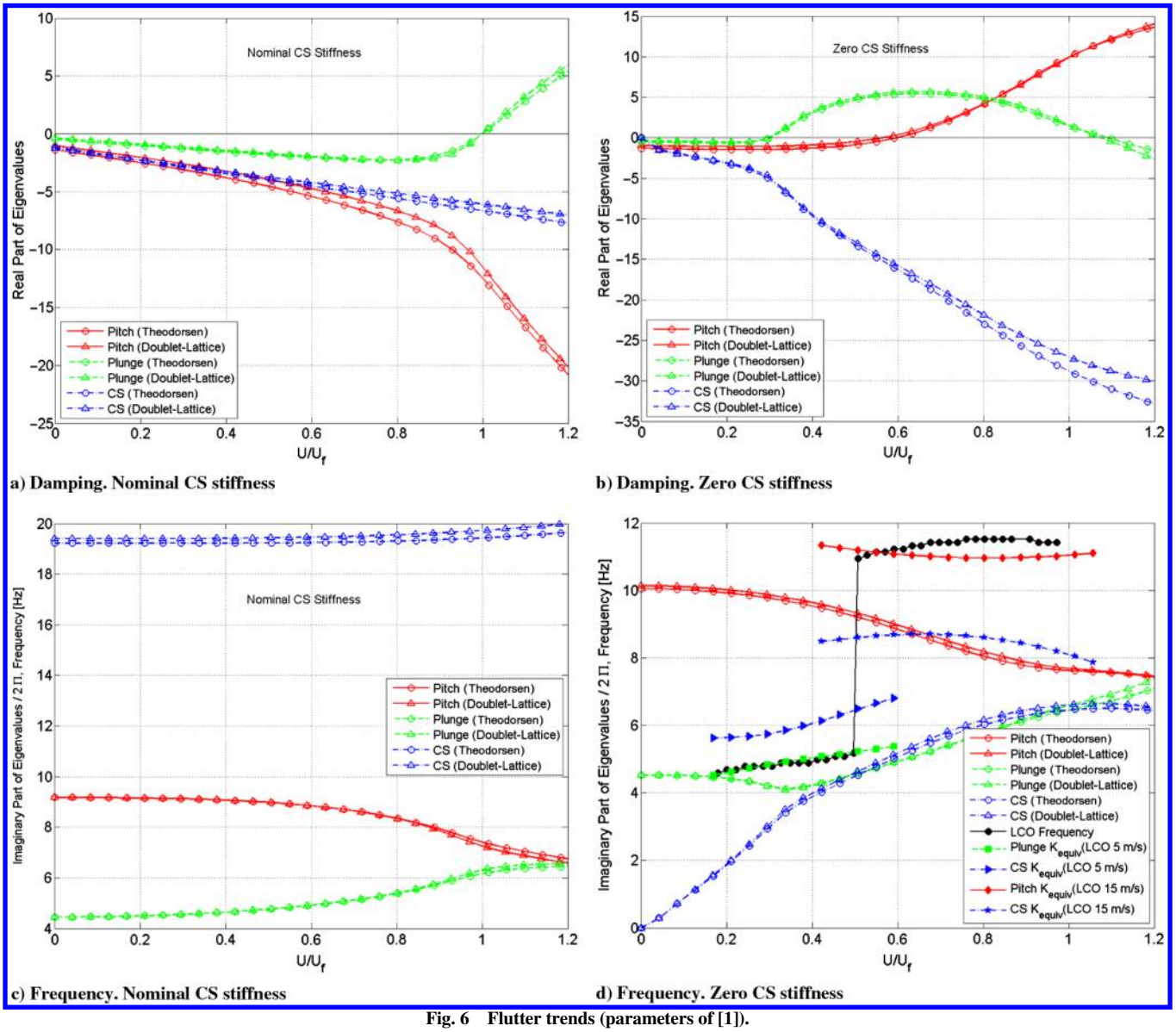

Fig. 6 Flutter trends (parameters of [1]).

character of the quasi-periodic oscillations present in the transition region."

These changes in the response may appear unexpected. For example, Trickey et al. [10] write, "Clearly, the situation is considerably more complicated than the underlying linear system response, which consists of stationarity followed by unlimited divergence". The flutter and aeroelastic frequencies of this (nominal, i.e., without freeplay) system are shown in the left part of Fig. 6. The situation is not considerably more complicated, however, if as the underlying linear system one considers the other linear system present in this problem. That system is the system with zero CS rotational stiffness, and its flutter trends are shown in the right part of Fig. 6. It is hoped that the following discussion that makes use of the flutter trends of the two linear systems shown in Fig. 6 can contribute to the explanation behind the changes in the response.

The CS is dynamically unbalanced, and so when its rotational stiffness is zero, it may flutter. During the motion, when the CS rotation exceeds the freeplay, the nominal linear system then stabilizes or limits the oscillations. This process results in the LCO of the nonlinear system. In the considered model, the nominal system becomes also unstable at U_f albeit for a completely unrelated reason, the main surface pitch-plunge flutter. At that point, the nominal system extracts the energy from the flow, and the otherwise limited oscillations diverge. Note that, because the fully operative aircraft is flutter-free in the expanded flight envelope, the CS LCO would not diverge inside the envelope. Examining the flutter trends shown in the right part of Fig. 6, one can observe the following. As the airspeed is increased, the aerodynamically stiffened CS couples with the plunge mode that has the lowest frequency of the two remaining modes. The outcome is 4.2 Hz flutter at $U \approx 0.3U_f$. The LCO of the nonlinear system can be expected to have a similar frequency and to be plunge-dominated. At $U \approx 0.6U_f$, while still interacting with the plunge mode, the further stiffened CS couples with the 8.9 Hz pitch mode as well. Therefore, it would not be unreasonable to expect the nonlinear system to exhibit a more complex response and for the initial conditions to play a role in the bias of the oscillations to either of the pitch or plunge-dominated motions. As the airspeed is increased more, the instability of the pitch mode begins to dominate until finally, at $U \approx 1.07U_f$, the CS and plunge modes decouple; thus, one can expect a drop in the LCO plunge amplitude and the LCO to be pitch dominated.

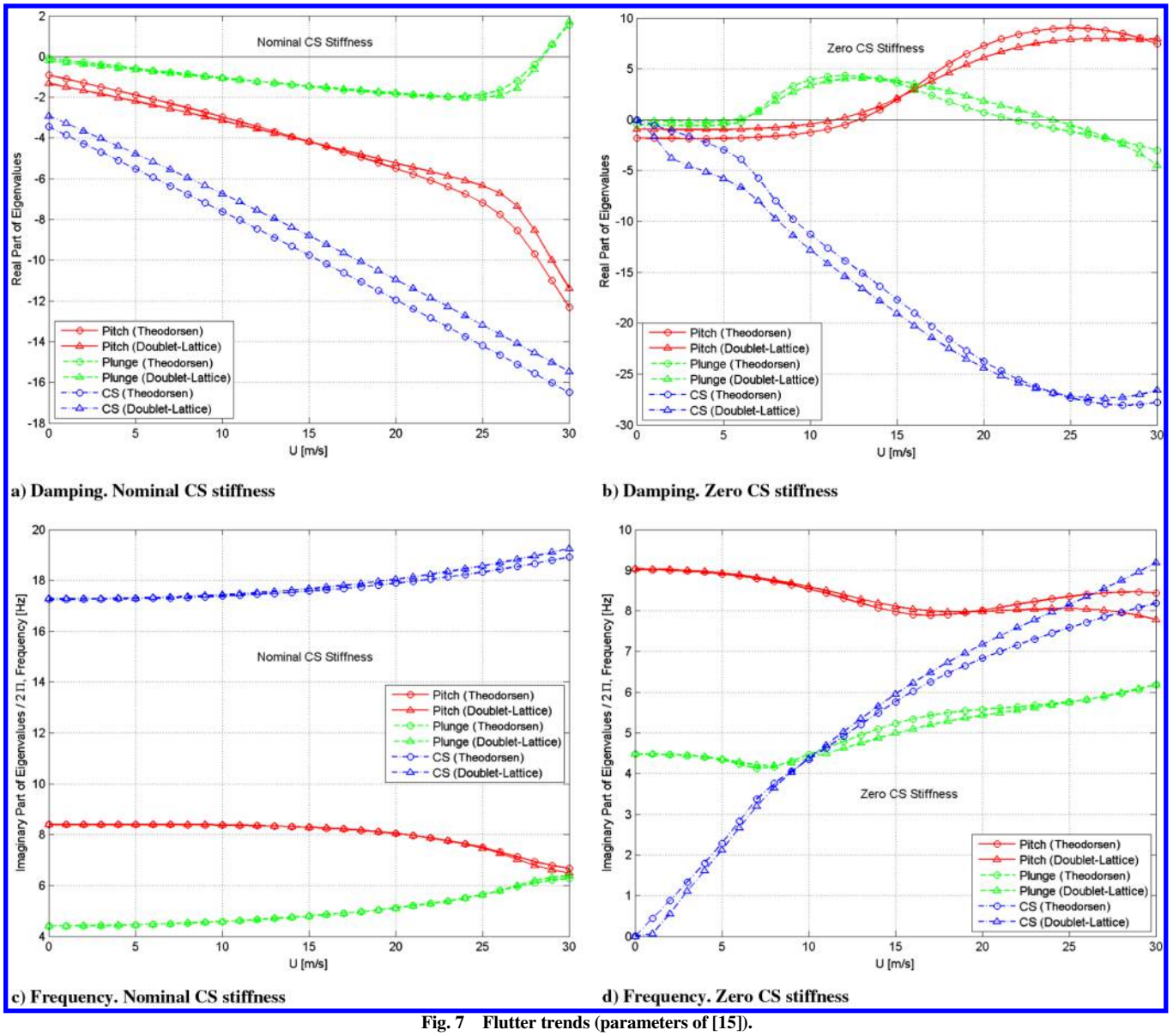

Fig. 7 Flutter trends (parameters of [15]).

Even though quantitatively the values of the LCO bifurcation airspeeds and frequencies from Fig. 4 do not agree well with the previous values, the flutter trend plot of the zero CS stiffness linear system does provide a preview of the LCO behavior. In fact, had the LCO amplitude been limited by the freeplay exactly, and therefore the CS stiffness were equal to zero throughout the cycle, the quantitative agreement would have been significantly better. Furthermore, as it has been shown for example in [4,9,12], one can use the DFM or HBM to determine the equivalent CS stiffness of a linear system from the knowledge of the LCO amplitudes of the nonlinear system. Then, not only can flutter trends of a linear system give a qualitative description of the situation, but some quantitative agreement can be observed as well. In Fig. 6d, also presented are the LCO frequencies from Fig. 4 and the eigenvalues for two "equivalent" systems. In one of them, the CS stiffness corresponds to the CS LCO amplitude at 5 m/s (only the plunge and CS modes are shown in Fig. 6d), and in the other, the CS LCO amplitude was taken at 15 m/s (the pitch and CS modes are shown). Note how well the plunge and pitch frequencies of these two system match with the LCO frequencies. The pitch dominated LCO frequency prediction can be further improved, of course, if instead of using only one (15 m/s) airspeed, the LCO amplitude used for obtaining the equivalent system was obtained at all corresponding airspeeds (from ~15 to 23.65 m/s).

As the CS LCO amplitude grows in Fig. 4, so does the equivalent stiffness, and that is why the eigenfrequencies of the equivalent linear systems in Fig. 6d move up, "jump" over the plunge mode frequency, and "push" the pitch mode frequency up. For the equivalent system corresponding to the CS LCO amplitude at 15 m/s, there is only one flutter mechanism, CS pitch, that begins at ~13m/s ($U \approx 0.55U_f$), which is where "the low-frequency limit cycle suddenly becomes unstable, and the system is attracted to a stable, high-frequency limit cycle" [12]. The "dramatic drop in the plunge amplitude at this point" is due to the plunge mode no longer "fluttering" but oscillating as part of the complete coupled system. This is not shown in Fig. 6, but the changes in the real part of eigenvalues as function of the equivalent stiffness are shown and discussed further in the nonzero preload section.

The same reasoning and especially the observation that higher LCO amplitudes may occur for higher equivalent CS stiffness is particularly helpful when examining the situation with nonzero aerodynamic preload or AoA of the CS. It will be shown that, once the effect of the preload or AoA on the CS rotational stiffness is accounted, one can return to flutter trends as shown in Fig. 6 to predict

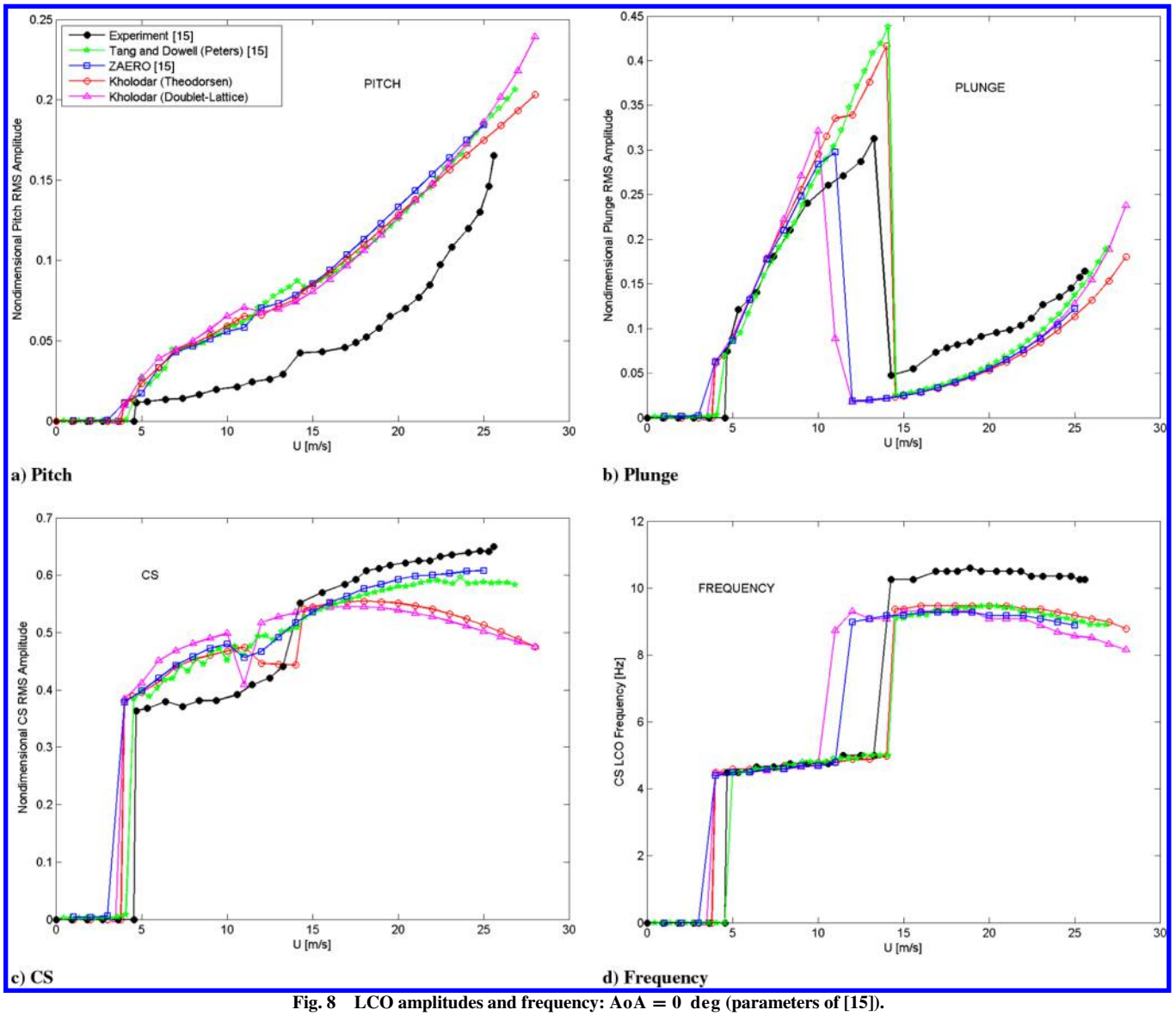

Fig. 8 LCO amplitudes and frequency: AoA = 0 deg (parameters of [15]).

what response of the nonlinear system to expect. However, before proceeding to that situation, consider Figs. 7 and 8 for the same system also at zero AoA but with the parameters of [15]. For the nominal system in Fig. 7a, again the two models predict similar flutter airspeeds: $U_f = 28.50$ m/s for the doublet-lattice model, and $U_f = 28.40$ m/s for the Theodorsen model ($U_f = 26.50$ in the experiment in [15]). For the zero CS rotational stiffness model, the two models predict different pitch flutter airspeeds: $U \approx 11$ m/s for the doublet-lattice model, and $U \approx 13$ m/s for the Theodorsen model. This explains why the transition to the pitch-dominated LCO occurs later in the Theodorsen model in Fig. 8.

Other factors such as the initial conditions and viscous damping do affect the LCO bifurcation airspeeds to some degree. This has been well discussed in previous publications and is not addressed here.

B. Nonzero Preload

Figures 8–12 present the experimental and theoretical results of Tang and Dowell [15] as well as the current results for AoA varying from 0 to 8 deg. Recall that $\delta = 4.24$ deg (Fig. 2b). The Theodorsen and doublet-lattice models yield adequate results that agree with the other two theoretical models. During the ground vibration test, an additional 11 Hz mode was observed. This "roll" mode appeared to be quite prominent, in fact, larger in magnitude of the transfer function than the nominal CS rotation mode [15]. Perhaps if the wing support asymmetries that lead to the occurrence of this mode are measured and modeled, the disagreement between the theory and the experiments can be improved. As also mentioned in [15], the main surface may experience nonlinear flow effects that are not modeled due to the AoA. For the detailed description of the results shown in Figs. 8–12, the reader is advised to read [15]. The conclusions reached in [15] with respect to the AoA study were provided in Sec. I.

An explanation to the behavior observed as the AoA is changed can be obtained by introducing another CS angle: preload δ_{PL} (Fig. 2b). The ratio δ_{PL}/δ is very important because it affects the CS rotational equivalent stiffness. For example, if for two different freeplay values δ, the preload is changed proportionally so that δ_{PL}/δ is kept the same, the LCO amplitude to freeplay ratio will stay the same. This explains the conclusion of [15] about the system response scaling with freeplay for nonzero AoA similar to zero AoA.

When the AoA is changed, the CS is forced to rotate to stay aligned with the airflow, and the CS equilibrium moves away from the middle of the freeplay. Shown in Fig. 13 is the variation of the preload with the airspeed and AoA obtained with the Theodorsen model by setting the viscous damping to very high, e.g., critical values (so that the static equilibrium of the system can be computed). For clarity, the preload at $U = 10$ m/s is shown on the inserted drawing in the top

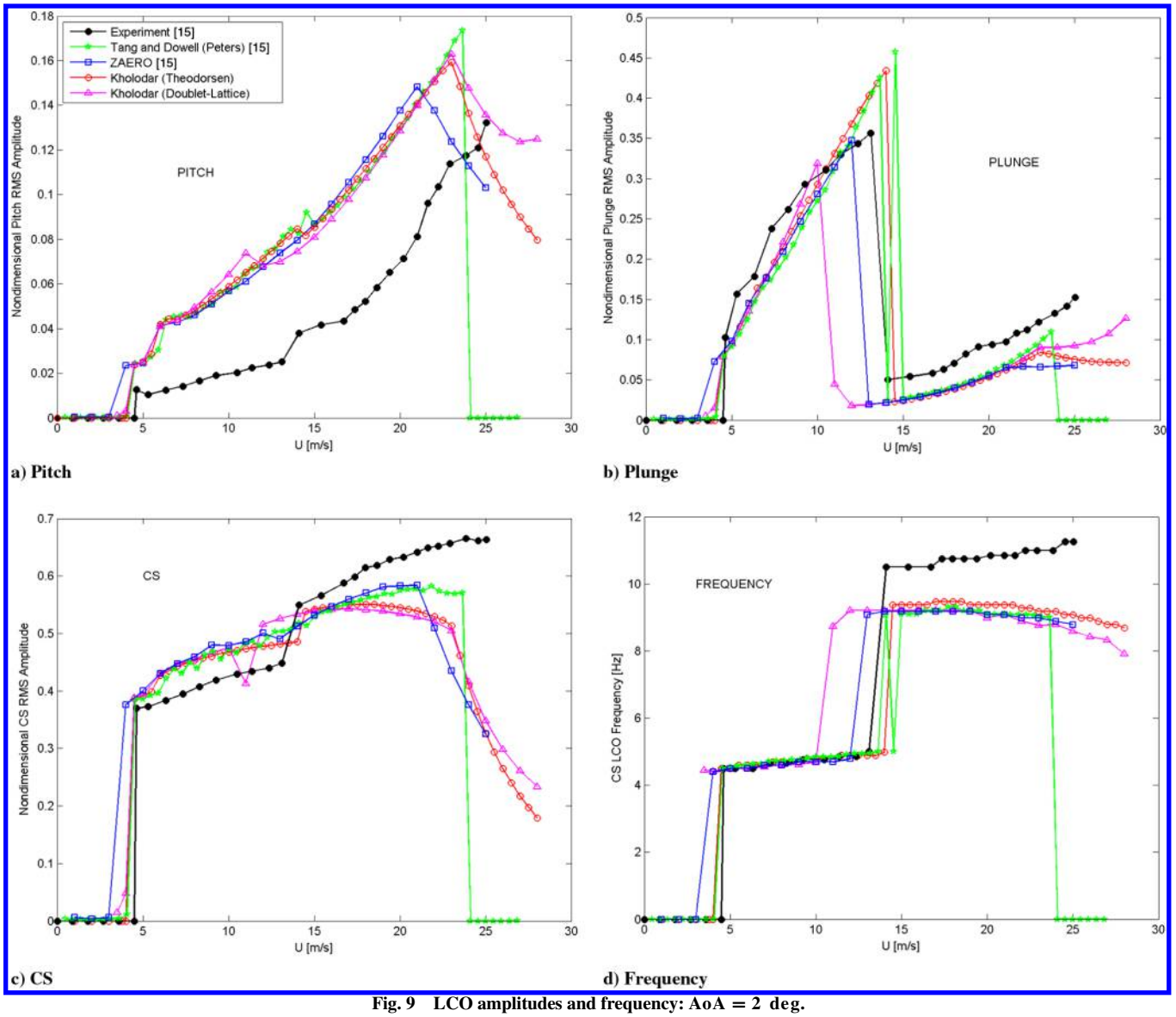

Fig. 9 LCO amplitudes and frequency: AoA = 2 deg.

left of the figure. Once the preload is known, one can use the frequency-domain methods such as the DFM and/or analyze the flutter trends to explain the behavior of the system similar to how it was done for zero AoA. For example, the equivalent stiffness obtained with the DFM for three preload values is shown in Fig. 14. As the preload grows, so does the equivalent stiffness and the CS rotational frequency. Figure 15 shows eigenvalues for zero and nonzero values of the equivalent stiffness. Note the lower flutter airspeeds of both modes in the case of the nonzero equivalent stiffness. This explains the conclusion of [15] about the occurrence of the higher-frequency (i.e., pitch) LCO at lower airspeeds with increased AoA. Another point about the equivalent stiffness in Fig. 14 is that, if one is inclined to rely exclusively on the DFM, he or she can use Fig. 14 and perform a freeplay analysis with nonzero preload similar to what was done in [4,12] for the case of zero preload. The Bombardier experience has been that it is beneficial to perform both time- and frequency-domain analyses. They compliment each other, reducing the time of the analysis and providing clarity of the interpretation. The total computational time for this study with two theoretical models is less than 10 min on a single personal computer.

The LCO amplitude variation at 10 m/s is shown in Fig. 16 as a function of AoA. The amplitudes are growing (albeit mildly) with the AoA in the experiments, despite the equilibrium position no longer being in the middle of the freeplay, and therefore the equivalent stiffness being higher. The same is true for the theoretical results (with the exception of the CS LCO amplitude that appears unchanged). For the preload associated with AoA larger than 8 deg, the LCO becomes quenched, as was also observed both experimentally and theoretically in [15]. The reason for the LCO amplitude growth is strengthening flutter. Consider again Fig. 6d or Fig. 15b. As the CS rotational frequency becomes higher with the preload growth, it moves closer to the frequencies of the other modes. The coalescence flutter responsible for the LCO could then strengthen on some airspeed intervals and weaken on the other. The flutter airspeed interval itself may become shorter or longer depending on the eigenfrequencies of the modes. In Figs. 8–12, for AoA > 2 deg, it began to become shorter. This explains the conclusion of [15] about the reduction of the LCO airspeed range for certain AoA. The increase in the CS rotational frequency above the other modes on the way to its fully operative position (Fig. 6c) eventually decouples the CS rotation mode from these modes, and the LCO become quenched. Such preload can be called the quenching or stabilizing preload.

For the system considered here, the LCO growth is minor. It can be larger for aircraft, especially in the transonic regime. Even more

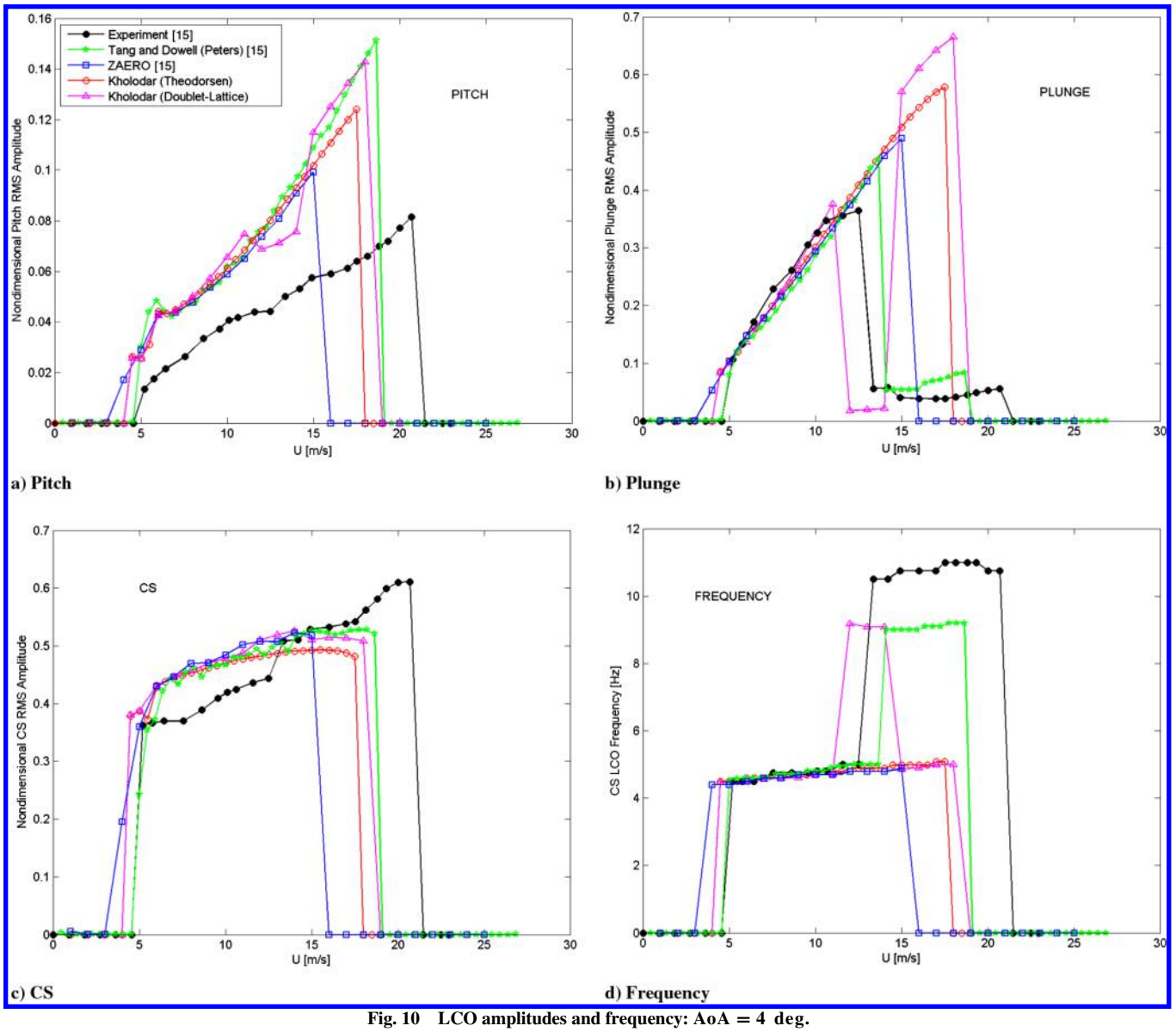

Fig. 10 LCO amplitudes and frequency: AoA = 4 deg.

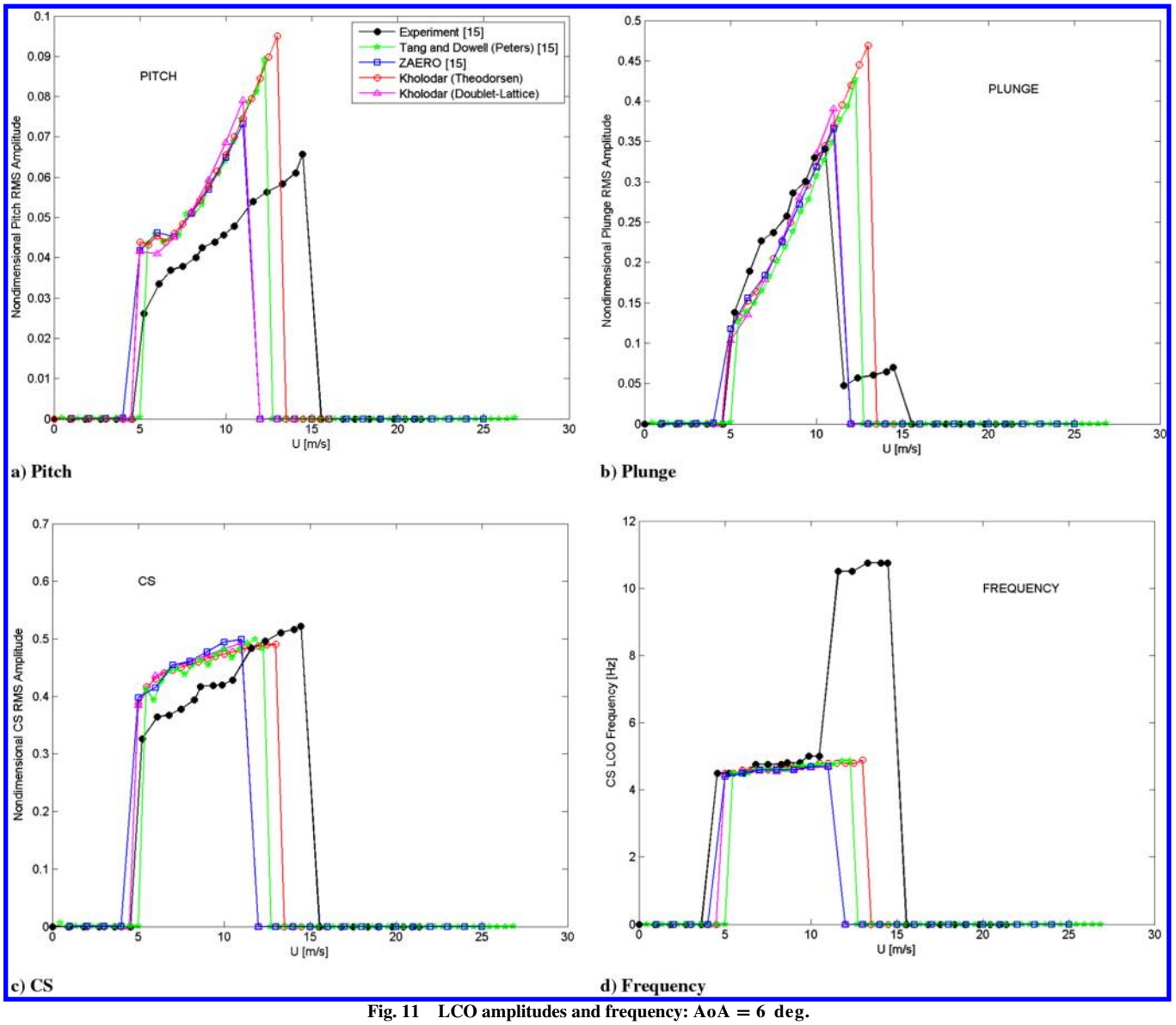

Fig. 11 LCO amplitudes and frequency: AoA = 6 deg.

importantly, in the aircraft case, there may be coupling of the CS rotation mode with modes that were not occurring at zero preload. This can manifest itself in, for example, an 18 Hz aileron LCO while the zero preload analysis had LCO frequencies in the range of 4 to 8 Hz. In perhaps another future publication on the subject, both of these points will be demonstrated.

An aircraft CS rotation mode is "placed" strategically by a judicious selection of the actuator stiffness. The implication of the preload effect is that the entire range of the CS rotation frequency between zero and the fully operative value must be considered for the potential LCO.

C. Suggestion for Future Experiment with Preload

A modification to the experimental freeplay model (see Fig. 2a) may be considered in the future. A device applying a hinge moment to the CS can be added. This is shown in Fig. 17. The aerodynamic nonlinearities associated with the nonzero AoA are then avoided. The preload becomes independent of the airspeed, and the experiment would permit determining the CS hinge moment that prevents the model from oscillating. Ultimately, an aircraft device providing a sufficient CS hinge moment can be designed. A simple example would be a bungee cord used on some aircraft to preload the rudder.

Finally, an experiment demonstrating that a certain preload is required to excite LCO that are otherwise not observed may be of value. To achieve that, there must be sufficient frequency separation between one of the high-frequency modes and the CS rotation mode so that they can only couple with a nonzero preload.

IV. Conclusions

The current study considered a well studied case of a three-degree-of-freedom aeroelastic wing with control-surface freeplay nonlinearity and varying angles of attack. Two theoretical models of the structure and aerodynamics were employed. The results presented were compared with the experimental and other published theoretical data.

The dynamic response in general was presented as dependent on 1) the stability of two linear systems (one with zero control-surface rotational stiffness and the other with the nominal stiffness), and 2) the values of two angles (freeplay and preload).

A physical explanation was given to the bifurcation airspeeds and oscillation frequencies for the system with both zero and nonzero preload. This was accomplished by examining the flutter trends of the aforementioned and other equivalent linear systems present in the nonlinear system. Excellent agreement between the eigenfrequencies

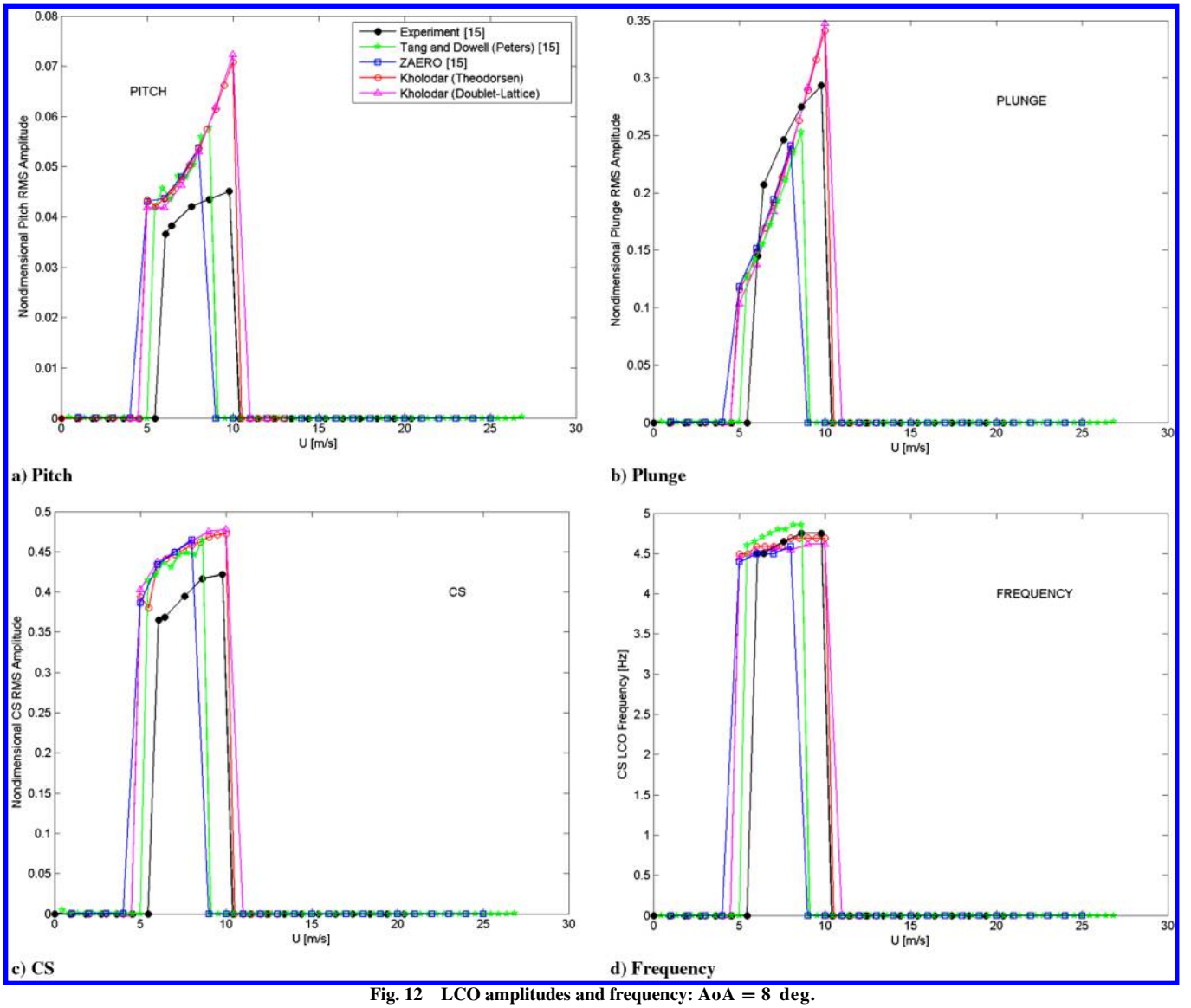

Fig. 12 LCO amplitudes and frequency: AoA = 8 deg.

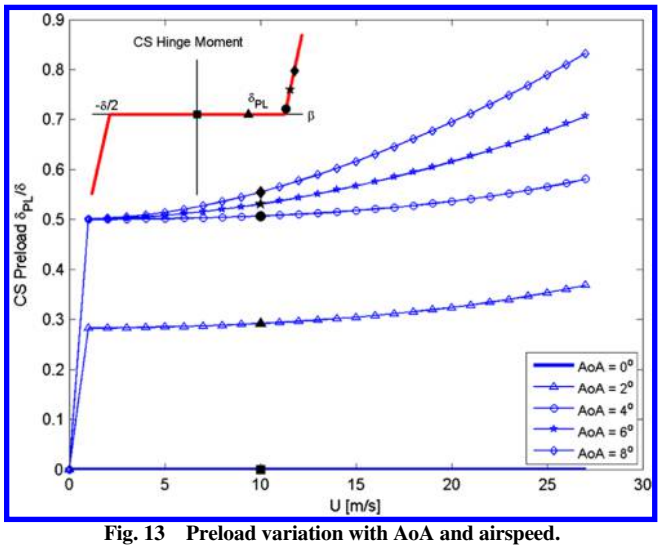

Fig. 13 Preload variation with AoA and airspeed.

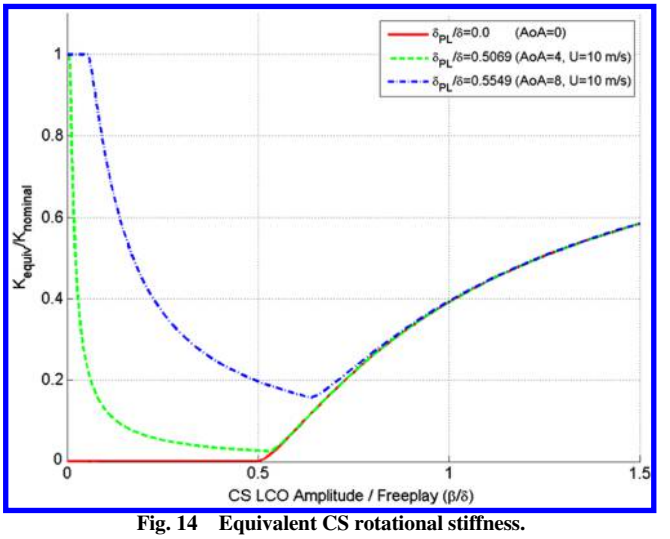

Fig. 14 Equivalent CS rotational stiffness.

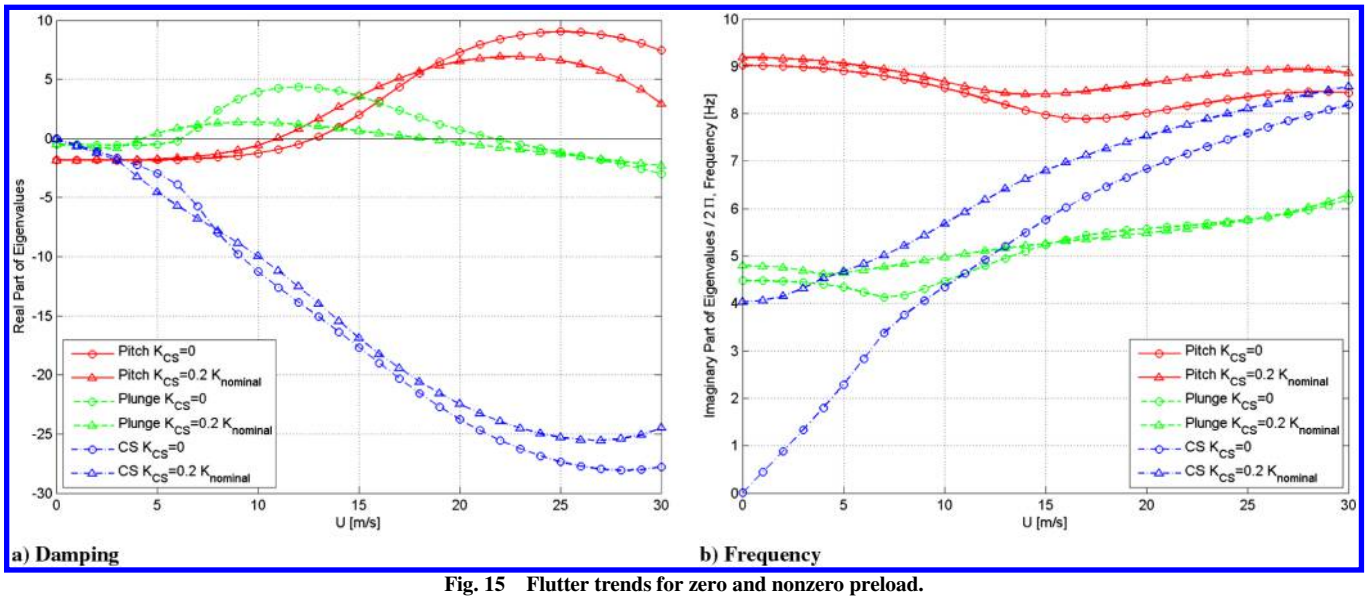

Fig. 15 Flutter trends for zero and nonzero preload.

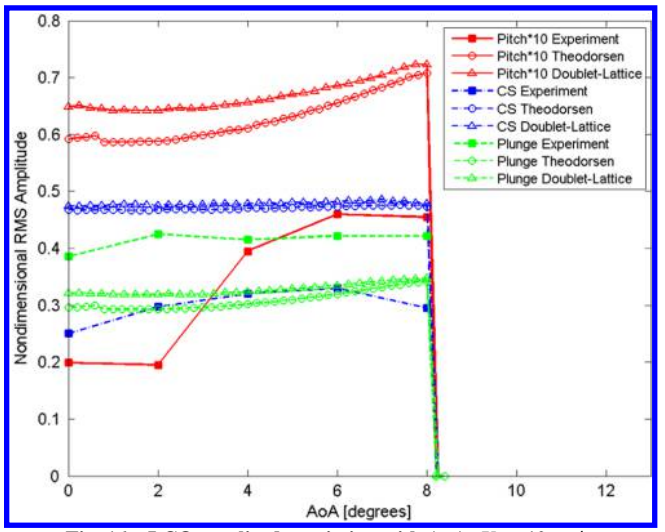

Fig. 16 LCO amplitude variation with AoA: $U = 10$ m/s.

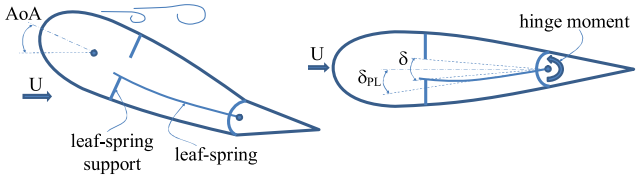

a) Preload due to angle of attack b) Preload due to CS hinge moment

Fig. 17 Creating preload angle δ_{PL} experimentally.

of the flutter modes in these systems and LCO frequencies was observed.

In the case of nonzero control-surface preload or angle of attack, it was shown why a certain amount of the preload is destabilizing and can also lead to the otherwise unexpected higher-frequency oscillations. The physical reason behind this is the increase of the equivalent rotational stiffness of the control surface. These findings imply that aircraft control-surface freeplay analyses based only on zero and substantially high aerodynamic preloads are nonconservative.

Finally, modifications to the model were suggested for future experiments, with the goal to study the effect of the preload and determine the stabilizing hinge moment. Technologies developed in such experiments would permit to ensure the absence of aircraft freeplay-induced LCO.

References

[1] Conner, M. D., Tang, D. M., Dowell, E. H., and Virgin, L. N., "Nonlinear Behavior of a Typical Airfoil Section with Control Surface Freeplay: A Numerical and Experimental Study," *Journal of Fluids and Structures*, Vol. 11, No. 1, 1997, pp. 89–109. doi:10.1006/jfls.1996.0068

[2] Theodorsen, T., "General Theory of Aerodynamic Instability and the Mechanism of Flutter," NACA Rept. 496, 1935.

[3] Edwards, J., Ashley, H., and Breakwell, J., "Unsteady Aerodynamic Modeling for Arbitrary Motions," *AIAA Journal*, Vol. 17, No. 4, 1979, pp. 365–374. doi:10.2514/3.7348

[4] Tang, D., Dowell, E. H., and Virgin, L. N., "Limit Cycle Behavior of an Airfoil with a Control Surface," *Journal of Fluids and Structures*, Vol. 12, No. 7, 1998, pp. 839–858. doi:10.1006/jfls.1998.0174

[5] Peters, D. A., and Johnson, M. J., "Finite-State Airloads for Deformable Airfoils on Fixed and Rotating Wings," *Proceedings of the Symposium on Aeroelasticity and Fluid/Structure Interaction*, American Society of Mechanical Engineers, Fairfield, NJ, Nov. 1994, pp. 1–28.

[6] Peters, D. A., and Cao, W. M., "Finite State Induced Flow Models Part 1: Two-Dimensional Thin Airfoil," *Journal of Aircraft*, Vol. 32, No. 2, 1995, pp. 313–322.

[7] Chen, P. C., and Sulaeman, E., "Nonlinear Response of Aeroservoelastic Systems Using Discrete State–Space Approach," *AIAA Journal*, Vol. 41, No. 9, 2003, pp. 1658–1666. doi:10.2514/2.7311

[8] Roger, K. L., "Airplane Math Modeling Methods for Active Control Design," AGARD CP-228, 1977, pp. 1–11.

[9] Liu, L., and Dowell, E. H., "Harmonic Balance Approach for an Airfoil with a Freeplay Control Surface," *AIAA Journal*, Vol. 43, No. 4, 2005, pp. 802–815. doi:10.2514/1.10973

[10] Trickey, S. T., Virgin, L. N., and Dowell, E. H., "The Stability of Limit-Cycle Oscillations in a Nonlinear Aeroelastic System," *Proceedings of the Royal Society of London, Series A: Mathematical and Physical Sciences*, Vol. 458, No. 2025, 2002, pp. 2203–2226. doi:10.1098/rspa.2002.0965

[11] Kuruvila, G., Bartels, R. E., Hong, M. S., and Bhatia, K. G., "Nonlinear Aeroelastic Analysis Using a Time-Accurate Navier–Stokes Equations Solver," *Proceedings of the International Forum on Aeroelasticity and Structural Dynamics (IFASD)*, 2007, pp. 1–14.

[12] Gordon, J. T., Meyer, E. E., and Minogue, R. L., "Nonlinear Stability Analysis of Control Surface Flutter with Free-Play Effects," *Journal of Aircraft*, Vol. 45, No. 6, 2008, pp. 1904–1916. doi:10.2514/1.31901

[13] Woolston, D. S., Runyan, H. L., and Anrews, R. E., "An Investigation of Effects of Certain Types of Structural Nonlinearities on Wing and

Control Surface Flutter," *Journal of the Aeronautical Sciences*, Vol. 24, No. 1, 1957, pp. 57–63.

[14] Chen, P. C., and Lee, D. H., "Flight-Loads Effects on Free-Play Induced Limit Cycle Oscillation," *47th AIAA Structures, Structural Dynamics, and Materials Conference*, AIAA Paper 2006-1851, May 2006.

[15] Tang, D., and Dowell, E. H., "Aeroelastic Airfoil with Free Play at Angle of Attack with Gust Excitation," *AIAA Journal*, Vol. 48, No. 2, 2010, pp. 427–442.
doi:10.2514/1.44538

[16] MSC. Nastran, Software Package, Ver. 2008, MSC. Software Corp., Santa Ana, CA, 2008.

[17] Henon, M., "On the Numerical Computation of Poincaré Maps," *Physica D: Nonlinear Phenomena*, Vol. 5, Nos. 2, 3, 1982, pp. 412–414.